SPILITIZED PILLOW-HYALOCLASTITE SEQUENCE FROM ANDAMAN OPHIOLITE, INDIA: EMPLACEMENT AND ALTERATION IN A SUBMARINE ENVIRONMENT

Raymond A. Duraiswami*,✉, Aristle J. Monteiro*, Tahira N. Shaikh* and **Qazi Akhter****

* *Department of Geology, Savitribai Phule Pune University, Pune, India.*
** *University of Kashmir, Jammu and Kashmir, India.*
✉ *Corresponding author, e-mail: raymond.duraiswami@gmail.com*

Keywords: *pillows; hyaloclastite; sheet lavas; spilitization; ophiolite; South Andaman; India.*

ABSTRACT

The Corbyn's Cove area in south Andaman Island exposes a ~ 30 m thick sequence of sheet lavas, pillows and hyaloclastite deposits related to the Andaman Ophiolite, India. The upper sheet lavas are emplaced as tabular forms with thick, jointed core, vesicular crust and patchy hyaloclastite. The sheet lavas are criss-crossed by a network of calcite veins. The pillows constitute a modest flow field at the base of the sheet lavas and contain small (4.55 x 5.18 cm) to large (60.89 x 113.86 cm), spherical, non-vesicular, glassy entities. Pillow interiors contain radial and concentric joints. Absence of vesicles suggests that the pillows have been emplaced subaquaeously at depths greater than 4 km. The pillow lavas are fed by dykes. Thick hyaloclastite deposits containing sporadic patches of pillow breccias are intricately associated with the pillows in mound-like progradational bird foot deltas. In thin sections, the pillow lavas are characterized by lanceolate plagioclase and fretted pyroxene quenched morphologies in a holohyaline texture indicating high degrees of undercooling (ΔT ~ 100 to 200ºC). Plagioclase compositions range from Anorthite (An_{97-99}) in the core to Albite (An_{1-9}) in the glassy margin. Individual plagioclase phenocryst in the dyke and pillow interior show tabular forms (ΔT ~ 50ºC), with effects of albitization of the margin (An_{1-10}; S-D index - 1.89 to 65.57) and variable alteration in the core (PI - 20.84 to 37.14; CIA - 70.92 to 99.34). Geochemically, the dyke-pillow lavas are hypersthene-normative tholeiites that have undergone variable degrees of spilitization and alteration. The sheet lavas have higher concentrations of Cs, Rb, Ce, U, K, Sr, P, Zr and Yb relative to N-MORB due to post emplacement cryptic metasomatism related to the calcite stockwork. These episodes of alteration have influenced the mineralogy and geochemistry of the original lavas. The geochemistry of the lavas indicates that they were deposited in a MORB-like environment, with a possible back-arc affinity. We envisage that the entire sequence from Corbyn's Cove was emplaced subaqueously during the Late Cretaceous in the Indo-Sino Burmese sea along the flanks of a rising mid oceanic ridge where the magma (1222 to 1230°C; 6 to 8 kbar) was generated at shallow depths (~ 20 km) and erupted to the surface as dykes that fed the pillow lava flow fields. Spilitization of the pillow lavas to various degrees occurred at temperatures between 1218 to 1164ºC and even lower while the hydothermal alteration took place at temperatures well below 300°C.

INTRODUCTION

The Andaman and Nicobar Islands are located on the eastern edge of the Bay of Bengal, near the eastern margin of the Indian plate. They are a part of the Indo-Burma-Andaman microplate (Acharyya, 2007). They are the northernmost islands of the Sunda-Burmese arc, which extends from the Indonesian archipelago in the south to the Indo-Burma ranges in the north (Hamilton, 1978; 1979; Srivastava et al., 2004). To the west of the Andaman and Nicobar Islands lies the Java Trench (Fig. 1a), where the Indian oceanic plate is subducting beneath the Indo-Burma-Andaman microplate at a rate of 4 to 6 cm/yr (Curray, 2005). Ophiolites and associated siliclastic turbidites (Andaman Flysch Group, Pal et al., 2003; 2005) and continental clastics (Mithakhari Group, Karunakaran, 1968) are exposed in the eastern part of the south Andaman Islands (Fig. 1b). The lower part of the ophiolite suite consists of extensively serpentinized peridotites, while the upper part comprises ultramafic-mafic rocks, intrusive homogeneous gabbro-plagiogranite-dolerite with extrusive boninites and tholeiitic basalts (Pal and Bhattacharya, 2010; Ghosh et al., 2017; Bandyopadhyay et al., 2020).

Based on the continuity of morphotectonic, structural units and regional gravity anomalies, Acharyya (2007) inferred that the Andaman ophiolites form a part of the outer arc of ophiolite belt on the outer sedimentary island arc. Subsequent geophysical surveys have revealed a low gravity anomaly corresponding to a relatively less dense crust beneath the Andaman Islands (Subrahmanyam et al., 2008). Recently, seismic surveys also re-confirmed the presence of ~ 24 to 32 km thick, low density continental crust beneath the islands (Gupta et al., 2016). These important findings suggest that the Andaman Islands may bear an older Sino-Burmese continental keel that may have rifted along with Sumatra creating the Andaman Sea between them. Acharyya (2007) believed that the South Andaman ophiolite nappes propagated westward from the Eastern belt of the Indo-Burma Ranges and are related to the collision of the Burmese and the Indo-Burma-Andaman microcontinents. The exact tectonic significance and origin of the ophiolites exposed on the Andaman Islands is widely disputed, with some authors claiming them to have an N-MORB origin (Srivastava et al., 2004; Jaffri et al., 2010), while others associate them to supra-subduction (Acharyya, 2007; Ghosh et al., 2009; 2017; Bhattacharya et al., 2020; Bandyopadhyay et al., 2021). Some authors also propose a transitional origin between MORB and ocean island tholeiites (Ray et al., 1988). A back arc affinity has also been assigned to these ophiolites (Jaffri et al., 2010; Jafri and Sheikh, 2013; Ghosh et al., 2018). All of these interpretations are probably based soley on the geochemistry of rocks associated with the Andaman ophiolites.

The lavas associated with the South Andaman ophiolites are best exposed in and around Corbyn's Cove in the south Andaman Island (Fig. 1c). Barring a few studies (Jafri and Sheikh, 2013), the physical volcanology of the lavas including the pillow basalt-hyaloclastite relations from Corbyn's Cove are cursorily described. Other studies (e.g. Srivastava et al., 2004; Jafri et al., 2010) have relied extensively on the

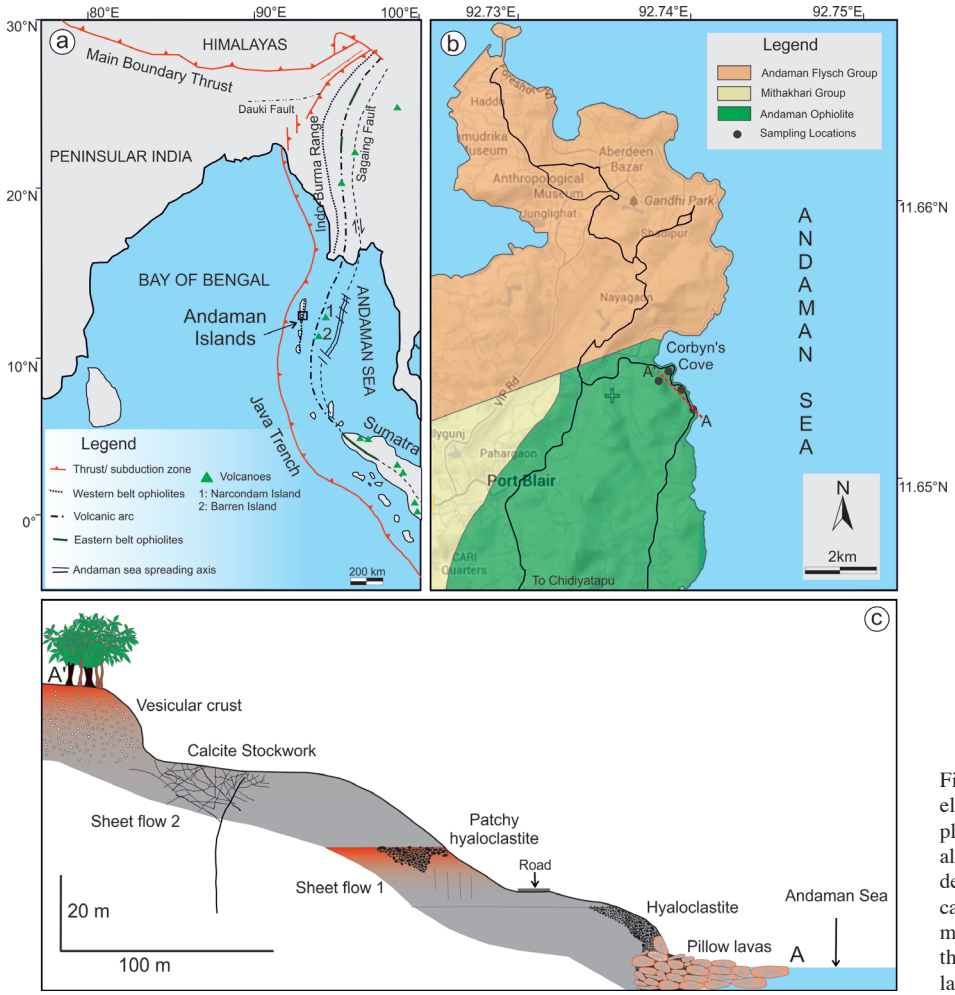

Fig. 1 - (a) Map depicting the various structural elements along the eastern margin of the Indian plate (modified after Acharyya, 2007 and Sheth et al., 2009). The black box near Andaman Islands denotes the approximate extent of b. (b) Geological map of the Corbyn's Cove area, South Andaman Island. (c) Schematic cross-section depicting the disposition of the pillow-hyaloclastite-sheet lavas in the Corbyn's Cove area.

geochemistry of the basaltic lavas for interpreting the tectonic setting and their petrogenesis. In the present study, we document the physical volcanology and field disposition of basaltic lavas and the pillow-hyaloclastite sequence from the South Andaman Island. We aim to study the mineralogy and textures present within the lavas in order to infer emplacement and cooling history. Lastly, we discuss the chemistry of the lavas *vis-à-vis* the lava-water interaction and alteration processes acting on them.

GEOLOGY OF THE CORBYN'S COVE AREA

In the South Andaman Island, thick sequences of sheet lava flows, pillow basalts and hyaloclastites are exposed in the hills immediately south of Corbyn's Cove beach (Fig. 1c). We describe their field occurrence, physical volcanology and morphometry in the following subsections.

Sheet lavas

In the hills south of Corbyn's Cove beach thick sheet lavas are exposed (Fig. 1c). The lava flow at the base ase fairly weathered (Fig. 2a), but preserve regular colonnade of subvertical cooling joints. Towards the upper parts of the lower lava sheet, pockets of coarse hyaloclastite are preserved. The hyaloclastite is characterized by unsorted, matrix-supported, glassy basaltic fragments. The fragments are of vesicular and massive varieties, some of which contain criss-crossing veins of calcite (Fig. 2b) suggesting veining prior to brecciation. Higher up in the section, a large quarry face exposes the upper thick lava sheet (Figs. 1c, 2c). Fresh vesicular basalt is exposed at the base of the quarry, while patchy yellow-green altered basalt is present above it. The upper quarry face is also characterized by criss-cross stockwork of calcite veins (Fig. 2d). The calcite veins are of at least two generations, several are displaced in an en-echelon pattern. In the proximity of the veins, the basalt appears to be chloritized.

Pillow lavas

To the south of the Corbyn's Cove section, pillow lavas are exposed in the wave-cut platform (Fig. 3a, b). Here, several hundred pillows constitute a flow field. Many pillows are bulbous and spherical in shape, but anastomosing, ginger-like interconnected pillow buds, toes and pillow branches are also common. Surfaces of individual pillows are rough, craggy (Fig. 3c) and show radial joints. Wherever exposed at the surface, or in cross-section, the pillows are sparsely vesicular; nearly all of them are devoid of pipes. Interestingly, the pillows do not show any longitudinal or transverse spreading cracks (Yamagishi et al., 1989). In places, 3-4 m long pillow tubes laterally feeding several bulbous toes and pillows are exposed in the wave-cut platform. Where slopes are steep, thin (30-40 cm) sheet lavas exist, the bases of which produce numerous large pillows (Fig. 3d). In exceptional cases, where

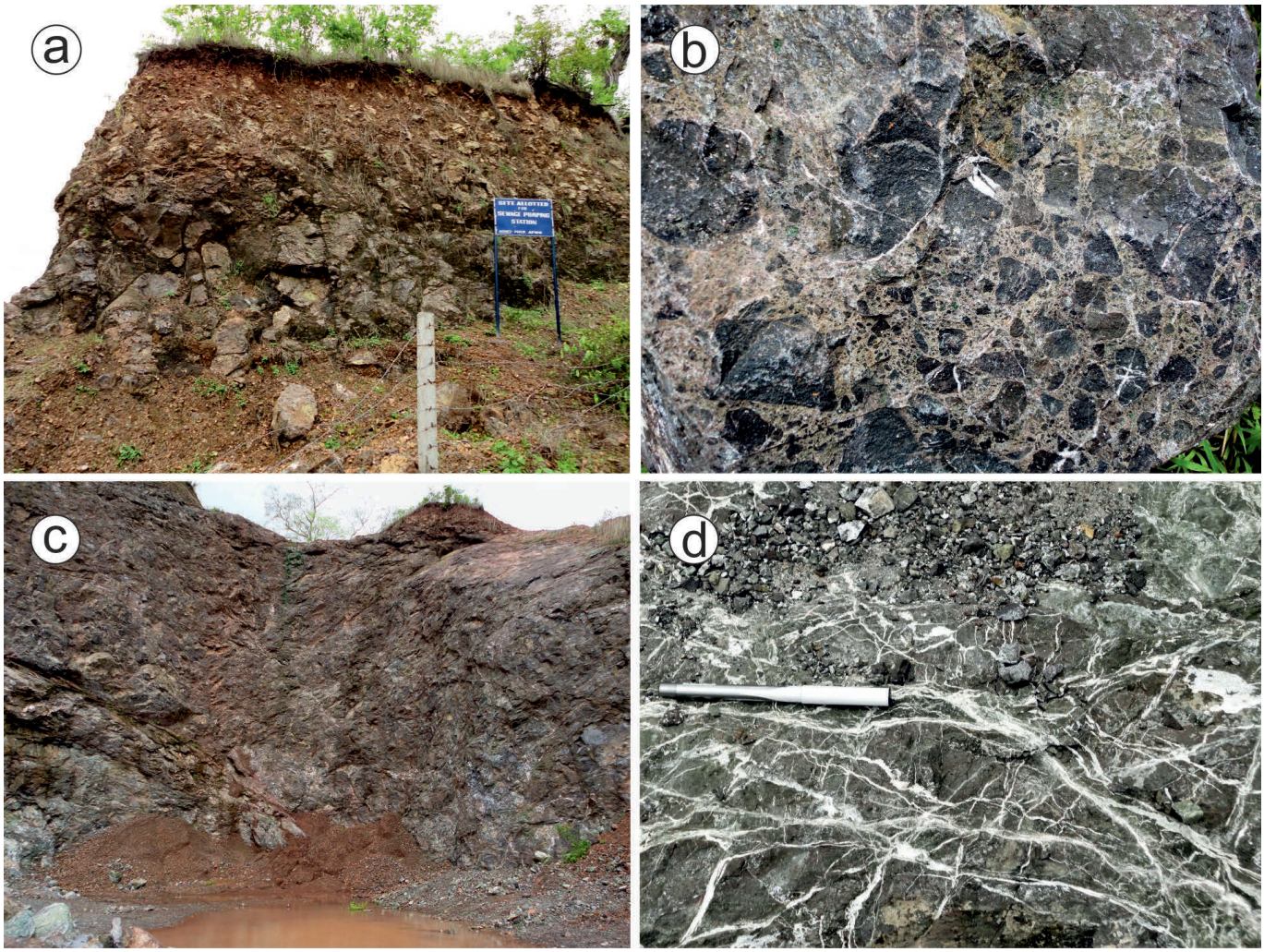

Fig. 2 - Field photographs depicting (a) sheet lava with regular colonnade jointing at the bottom. The upper portion of the sheet lava is weathered, and shows the development of a soil profile. (b) Glassy basaltic blocks within a matrix supported hyaloclastite. The basaltic fragments vary in size from around 2 cm to over 15 cm in length. (c) A quarry section exposing massive sheet lava. (d) Criss-crossing calcite veins seen in the basalt exposed in the quarry face.

slopes are greater than 7°C, large (~ 3 m long) singular elongated pillows are seen (Fig. S1). The inter-pillow spaces are generally empty (possibly removed by wave action), but seldom fine pillow breccia is preserved in a calcite matrix (Fig. 4a). Rarely, pillow breccias (Fig. 4b) accumulate and are preserved in discrete patches. In a majority of the cases, especially at the base of rocky cliffs, pillows are separated from each other by fine-grained, greenish-gray hyaloclastite (Fig. 4c). Seldom, stray ameboid pillows and elongated pillow tubes (in cross section) are preserved in thick fine-grained hyaloclastite deposits (Fig. 4d).

Towards the edge of the flow field, a small pillow delta-like feature is exposed (Fig. S2). The flow field here appears to dip steeply downslope and diverge into three distinct pillowed branches, where pillow elongations are seen towards the propagating front. In some branches, pillow breccia and pillow debris are common. The wave-cut platform also exposes thin dykes (Fig. 5). The dykes have curvilinear irregular contacts and their interiors are fine-grained, characterized by sparsely regular transverse cooling joints. Dyke margins are chilled, glassy and interiors contain few large vesicles concentrated towards the centre. The discordant relation of the dykes with the pillows is seen in several places, but elsewhere, the dykes appear to be feeding at least a couple of pillow lobes. It is speculated that the dykes could be contemporaneous with the pillows and thus fed at least a part of the pillow-sheet lava flow sequences at Corbyn's Cove.

To the extreme south of the pillow flow field, pillows are exposed in a ledge (Fig. 6a) and in the intertidal zone (Fig. 6b). Interestingly, the pillows here are made up of discrete bulbous entities that are separated by carbonates. Pillows here are spheroidal with smooth surfaces. Some of the pillows exhibit incipient turtle-shell jointing. In cross-section, the pillows are devoid of vesicles throughout. The pillows have developed a single thick glassy rim. The cores are fine-grained, homogenous and show well-developed radial and concentric jointing patterns (Fig. 6c). In places, interconnected reniform pillows are exposed in cross-section (Fig. 6d). The pillow lavas are criss-crossed by a stockwork of parallel to sub-parallel calcite veins.

Pillow - hyaloclastite association

Thick (2-5 m) hyaloclastite deposits (Fig. 1c) are exposed along the ledges of the wave-cut platform in the Corbyn's Cove area. These deposits occur as overhang delta-like fea-

Fig. 3 - Field photographs. (a) Outcrop of bulbous pillows to the south of Corbyn's Cove beach. (b) The other side of the outcrop. Most pillows in (a) and (b) are more or less equidimensional i.e. approximately spherical, though there are elongated pillows present at the bottom. Some of the pillows are connected to each other through buds. (c) Close-up view of bulbous pillows with a craggy surface. (d) Large pillows fed by thin sheet lava.

tures (Fig. S2) interdigitated with the underlying pillow lavas. Towards the south, large fan-shaped mounds are exposed (Fig. 7a). These deposits contain massive, unsorted, monolithic, clast-supported hyaloclastite (Fig. 7b). The deposits consist of small to large juvenile fragments of sub-angular to angular plag-phyric basalt, vesicular basalt and glassy quenched pillow fragments. In places, basaltic clasts exhibit dark glassy cores and seldom devitrify to a light greenish spilitic margin. The hyaloclastites also occur as discrete globular masses resembling phantom pillow forms. Towards the snout of the hyaloclastite deposits, coarser sub-rounded juvenile, glassy, massive and altered cobble-sized clasts tend to accumulate (Fig. 7c, d). In one of the toes of the bird-foot delta (Fig. S2), a fining up-sequence is recorded (Fig. 7e).

MATERIAL AND METHODS

The pillows from the south Andaman Island were studied and measured in the field for their geometries similar to the work previously conducted by Walker (1992) and Duraiswami et al., (2013; 2019). A total of fifty pillows were measured from Corbyn's Cove beach along the horizontal (H) and vertical (V) dimensions, parallel and perpendicular to the assumed surface at the time of emplacement of these pillows. The data are presented in Table S1 and the summary of their statistics are presented in Table 1.

Samples from pillow lavas, hyaloclastites and a single dyke were collected from the field after ensuring that they were relatively fresh, and thin sections were prepared from

Table 1 - Statistics of the distribution of horizontal axis (H) and vertical axis (V) of the measured pillow dimensions in the study area.

	H (cm)	V (cm)
Number	50	50
Minimum	5.18	4.55
Maximum	113.9	60.89
Average	30.04	18.31
Median	24.62	15.64
Standard Deviation	20.01	11.36
Skewness	1.72	1.77

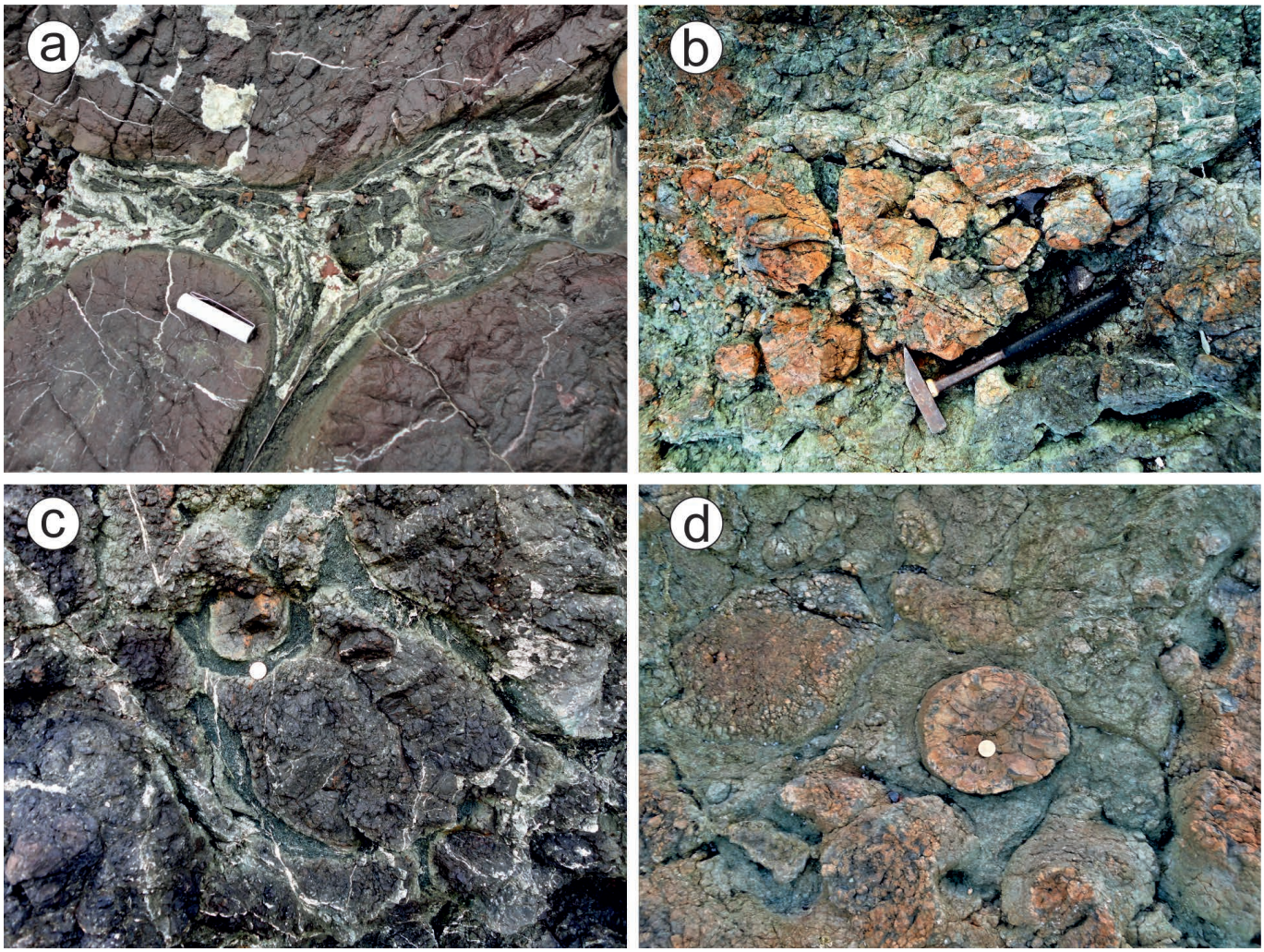

Fig. 4 - Field photographs depicting (a) Pillow breccia with a calcite matrix within the inter-pillow spaces. (b) Accumulation of pillow breccia, occurring as a discrete patch within hyaloclastite. (c) Greenish-gray hyaloclastite within the inter-pillow spaces. (d) Pillow tube in the centre preserved within fine-grained hyaloclastite. Also note the presence of ameboid-shaped pillows to the bottom and right of photograph.

these samples in order to study their mineralogy and textures under a Nikon research microscope at the Department of Geology, Savitribai Phule Pune University. Apart from this, Electron Probe Micro Analysis (EPMA) of some minerals in polished section was undertaken at the Indian Institute of Technology Bombay, in order to identify the type of plagioclase and pyroxenes and study the variations in mineral chemistry. The chips of representative rocks samples were washed thoroughly with ultrapure water, crushed and powdered using an agate mortar and pestle. In total, 6 samples, three from sheet lava (CC, CC1, CC5) two pillow basalts (CCPB, CCPB3), and one dyke (CCD1) were analyzed for their major and trace elements using X-ray fluorescence and ICP-MS respectively at the National Geophysical Research Institute (NGRI), Hyderabad. Normative mineral compositions were calculated using the major element oxides using SINCLAS (Verma et al., 2002). The major element compositions, along with the normative mineralogy, for the samples are presented in Table 2 while the trace element concentrations are presented in Table 3. The magmatic temperature was constrained using whole rock + pyroxene compositions (Putirka et al. 1996; Putirka, 2008), single pyroxene composition only after Nimis and Taylor (2000) and Putirka (2008). In these models, most thermometers are P-sensitive and most barometers are T-sensitive. Two equations can be solved simultaneously to arrive at P and T, which is accomplished here by using the output of one model as input for another. The studied samples do not contain any pressure sensitive mineralogy that can be used to constrain emplacement pressure. Moreover, the pillow lavas indicate very low pressures of emplacement and crystallization (subaqueous emplacement). Hence, we do not report the estimated pressures. Tests for equilibrium between clinopyroxene and a nominal coexisting liquid was made by comparing observed and predicted values for Fe-Mg exchange, or $K_D(Fe\text{-}Mg)^{cpx\text{-}liq}$, which should be 0.27±0.03. We used K_D (Fe-Mg) of ~ 0.29 for the dyke and higher K_D's of ~ 0.31 (CCPB3) and ~ 0.48 (CCPB). These clearly indicate the dyke represents magmatic temperatures while the pillows record temperatures at which spilitization occurred.

RESULTS

Pillow morphometry

The mean length of the pillows from Corbyn's Cove along the H-axis was 30.4 cm (with a standard deviation of 20.21 cm), while along the V-axis, the mean size was 18.31 cm (standard deviation of 11.47 cm). The smallest pillow

Table 2 - Major oxide (wt.%), CIPW normative mineralogy and other ratios of samples from the present study.

	Sheet lavas			Pillow lavas		Dyke
Sample	CC	CC1	CC5	CCPB	CCPB3	CCD1
Rock type	TB, pot	TB, pot	B, subal	B, alk	B, subal	B, subal
SiO_2	48.15	47.52	48.75	47.91	49.56	49.59
TiO_2	1.43	1.49	1.1	1.37	1.18	1.05
Al_2O_3	17.05	17.44	19.25	14.74	16.19	15.02
FeO_T	11.96	12.12	9.48	10.14	8.82	9.63
MnO	0.18	0.18	0.15	0.17	0.16	0.15
MgO	3.86	3.84	4.34	6.23	6.86	8.66
CaO	8.5	8.47	10.23	12.25	10.27	9.51
Na_2O	3.24	2.93	2.54	2.99	3.25	2.96
K_2O	1.66	1.94	1.04	0.38	0.62	0.61
P_2O_5	0.28	0.33	0.14	0.13	0.11	0.09
Total	96.32	96.26	97.01	96.3	97.01	97.27
CIPW norms						
Or	10.12	11.86	6.31	2.31	3.75	3.7
Ab	28.42	25.67	22.09	24.91	28.32	25.74
An	28.02	29.75	39.17	26.62	28.56	26.56
Ne	-	-	-	0.72	-	-
Di	11.45	9.65	10.04	29.15	18.84	17.27
Hy	4.61	4.89	15.1	-	5.46	10.91
Ol	9.64	10.15	2.4	10.71	10.28	11.14
Mt	4.24	4.3	2.4	2.58	2.23	2.43
Il	2.82	2.94	2.16	2.69	2.3	2.04
Ap	0.68	0.79	0.34	0.32	0.26	0.21
Mg#	42.2	41.78	49.07	56.37	62.06	65.4
FeO_T/MgO	3.1	3.16	2.18	1.63	1.29	1.11
Salic	66.56	67.29	67.57	53.84	60.63	56.00
Femic	26.58	26.69	27.18	33.15	32.39	38.09
CI	44.65	44.78	56.37	69.36	63.12	63.25
DI	38.54	37.53	28.4	27.93	32.07	29.44
SI	18.37	18.19	24.73	31.29	34.83	39.3
AR	1.47	1.46	1.28	1.29	1.34	1.34
Weathering indices						
CIA	43.13	43.96	44.74	34.96	39.75	39.84
Parker	48.23	48.63	42.27	44.55	45.83	45.00
S-D	5.26	5.95	7.58	4.93	4.98	5.07

CIA = $[Al_2O_3/(Al_2O_3+CaO+Na_2O+K_2O)]x100$ Parker index = $(Na_a/0.35 + Mg_a/0.9 + K_a/0.25 + Ca_a/0.7)x100$

S-D index = Al_2O_3/Na_2O

Table 3 - Trace element concentrations (ppm) in samples from present study.

	Sheet lavas			Pillow lavas		Dyke
Sample	**CC**	**CC-1**	**CC-5**	**CCPB**	**CCPB-3**	**CCD-1**
Rock type	TB, pot	TB, pot	B, subal	B, alk	B, subal	B, subal
Sc	37.41	38.08	31.68	29.71	31.91	31.64
Cr	244	234.9	173	252.8	224.5	173.5
Co	40.77	38.56	35.59	32.47	35.37	35.68
Ni	95.94	98.57	64.68	88.45	79.72	112.3
Cu	25.11	21.65	43.19	56.19	32.75	60.85
Zn	97.83	96.24	85.72	71.78	94.82	81.01
Ga	16.98	18.01	17.12	15.29	15.84	14.67
Rb	78.52	72.48	48.17	12.18	17.61	14.05
Sr	238.8	240.6	174	166	180.5	209.3
Y	36.11	41.72	34.5	34.51	38.71	31.67
Zr	140.1	150.7	116.5	127.1	139.8	150.8
Nb	2.007	1.722	5.064	1.451	2.871	1.221
Cs	1.848	2.198	1.024	0.098	0.171	0.23
Ba	141.3	166.1	106.6	34.53	45.69	36.71
La	4.08	4.47	5.4	3.43	4.47	2.83
Ce	20.75	21.08	20.48	18.35	23.28	15.23
Pr	1.79	1.93	1.6	1.42	1.79	1.19
Nd	7.99	8.49	6.97	6.44	7.96	5.37
Sm	3.63	3.89	2.75	2.74	3.28	2.35
Eu	1.31	1.37	1	0.93	1.11	0.83
Gd	4.33	4.62	3.12	3.06	3.67	2.72
Tb	1.05	1.15	0.72	0.74	0.86	0.67
Dy	8.55	9.38	5.46	5.64	6.57	5.16
Ho	2.37	2.71	1.45	1.49	1.73	1.37
Er	6.02	6.89	3.51	3.6	4.21	3.35
Tm	1.08	1.23	0.61	0.64	0.73	0.59
Yb	11.49	13.13	6.45	6.69	7.7	6.23
Lu	0.87	0.99	0.46	0.5	0.56	0.46
Hf	4.12	4.34	3.39	3.6	4.04	3.01
Pb	3.92	2.7	3.56	3.83	3.5	3.45
Th	0.15	0.27	0.22	0.2	0.21	-
U	0.29	0.19	0.13	0.16	0.16	-

TB: trackybasalt, B: basalt, pot: potassic, subal: subalkaline, alk: alkaline

Fig. 5 - Dyke exposed on the wave cut platform at Corbyn's Cove.

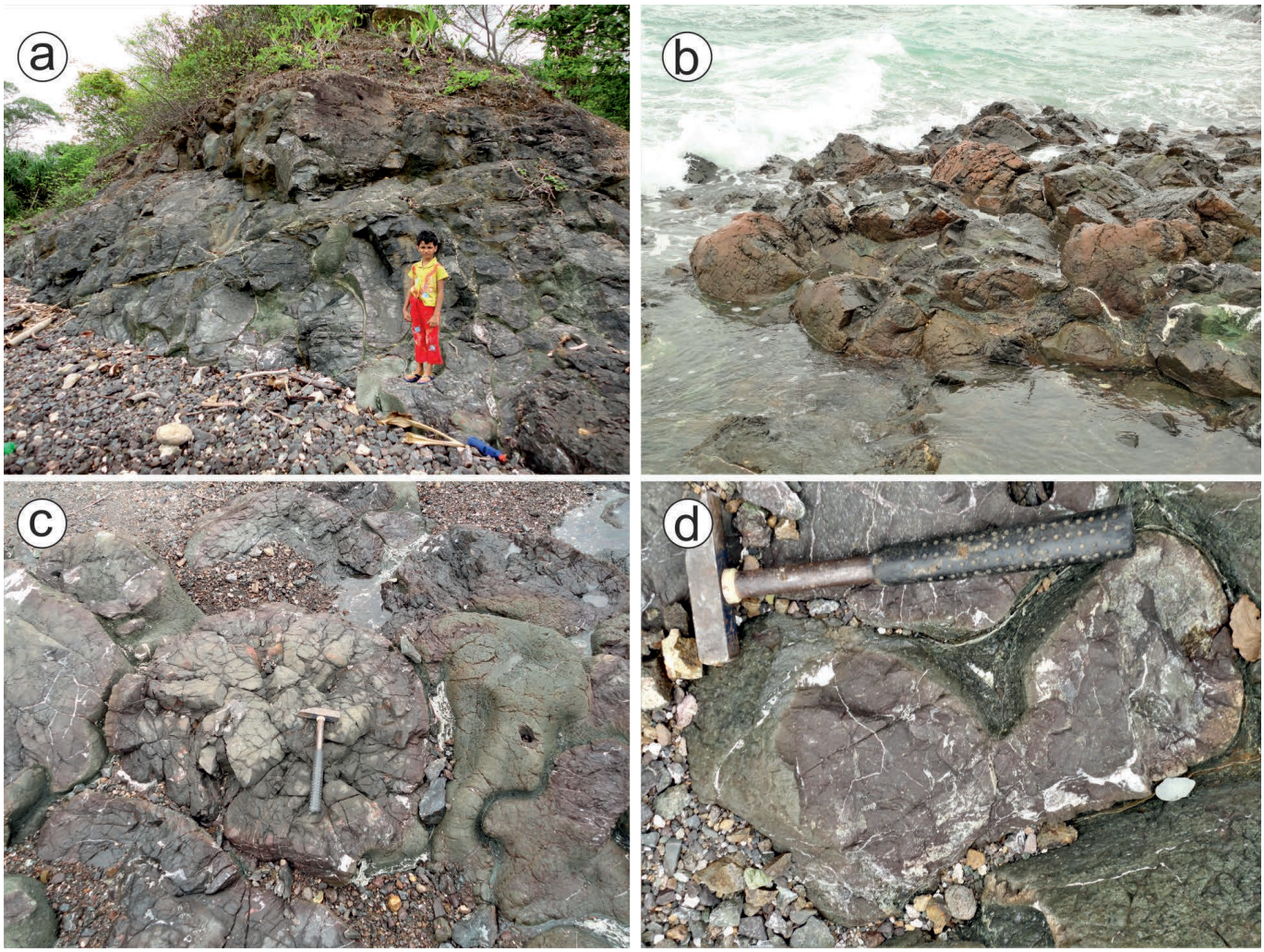

Fig. 6 - Field photographs. (a) Wave cut ledge exposing pillows in the field. (b) Pillow outcrop exposed along the wave cut platform. Individual pillow lobes are about 1 meter long. (c) Cross-section of pillow depicting well-developed radial jointing. A small elephant-trunk pillow with a smooth outer surface is also seen to the right of the photo. (d) Reniform pillow with fine-grained hyaloclastite within the inter-pillow spaces.

measured was 5.18 × 4.55 cm, while the largest pillow was 113.86 × 60.89 cm. A graph of the mean lateral dimension versus the mean vertical dimension was plotted to compare the pillow lavas from the present study with pillows from other Indian locations (after Duraiswami et al., 2013; 2019) and those measured by Walker (1992) from different locations all over the world. The mean dimensions of pillows from Corbyn's Cove are much smaller (Fig. S3) than those of Borivali, Chitradurga and Mardihalli, indicating either lower flow viscosity (Walker, 1992) or higher hydrostatic pressure at the time of emplacement. Absence of prominent vesiculation in the pillow interiors suggests deep emplacement of > 4 km (Moore, 1965; Duraiswami et al., 2013).

Petrochemistry

The pillow lavas exhibit large proportions of glass (~ 60 to 90%) and a variety of holohyaline textures (Fig. 8). The plagioclases from the pillow core occur as unzoned lath-shaped phenocrysts (Fig. 8a) and generally accumulate into glomeroporphyritic clots (Fig. 8b). These plagioclase crystals show varying degrees of resorption (Fig. 8c). Plagioclases in the groundmass most commonly appear as long and acicular crystals (Fig. 8d) with a swallow-tail morphology (Fig. 8e). In some pillows, earlier-crystallized plagioclase microphenocrysts act as sites for the heterogenous nucleation of plagioclase and pyroxenes. The latter occur as fretted and plumose skeletal crystals (Fig. 8e, f). Acicular quenched plagioclase crystals appear to curve or break when they come into contact with other plagioclase crystals. In thin sections, the pillow lavas also show incipient expansion cracks related to stretching (Fig. 9a). Pillow breccia fragments (Fig. 9b) formed after fracturing and brecciation along inflation creases are also common in thin sections. Intense brecciation due to criss-crossing fractures are also preserved (Fig. 9c). The individual breccia fragments are angular to subangular (Fig. 9d) and have quenched acicular plagioclase crystals set within a glassy groundmass. The pillow breccia appears distinctly different from hyaloclastite even in thin section, where angular juvenile glassy fragments are preserved in a calcareous matrix (Fig. 9e). Few basaltic fragments within the hyaloclastite have calcite veins passing through them (Fig. 9f), suggesting derivation from earlier formed sheet lava intruded by the calcite veins.

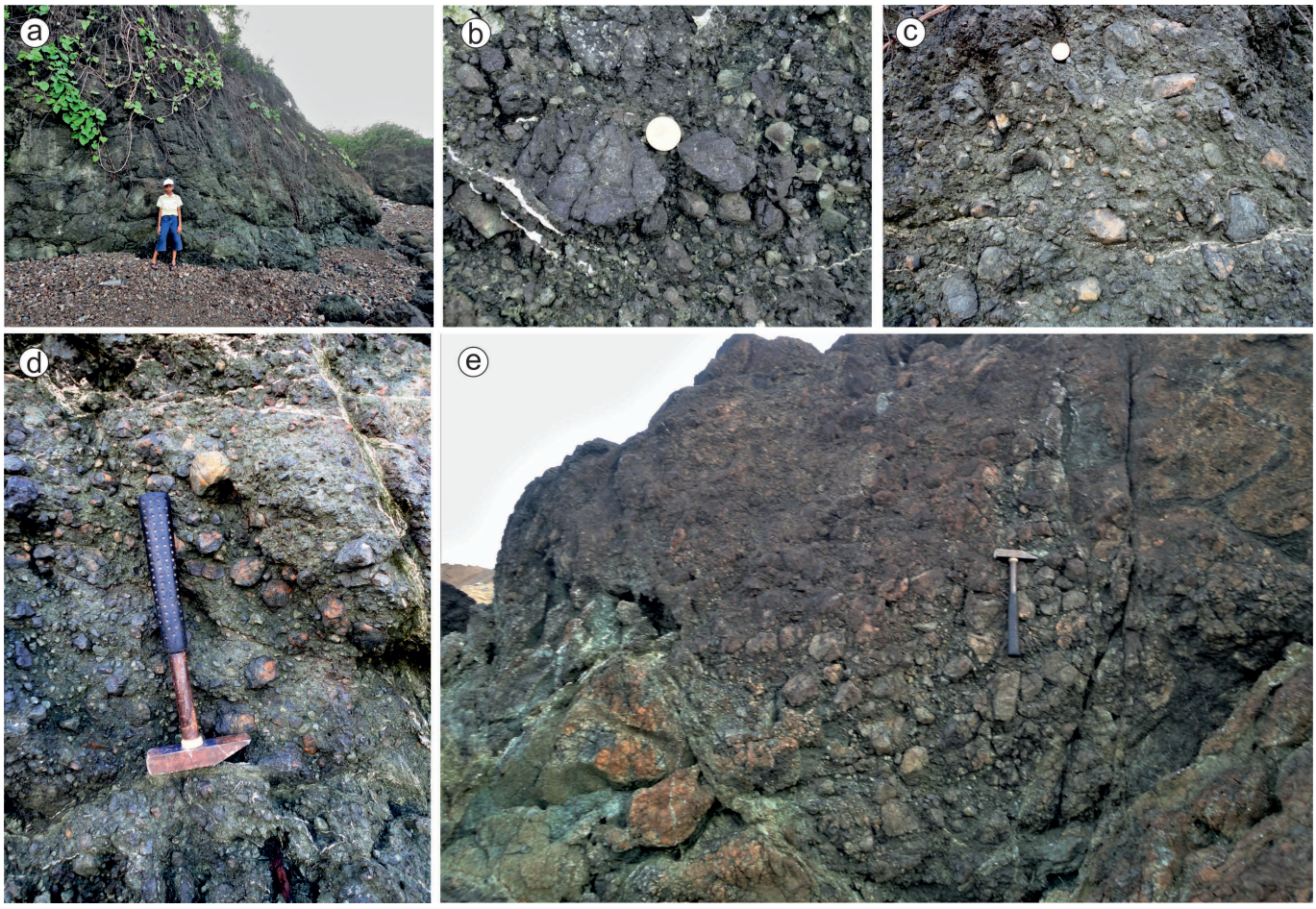

Fig. 7 - Field photographs depicting (a) a thick deposit of hyaloclastite overlying pillows. Note the mound-like character of the deposit. (b) Coarse-grained 'poorly sorted' hyaloclastite deposit with large pillow breccia fragment. Fragments of vesicular basalt, possibly from crust of overlying sheet flow, are also visible towards the top of the photograph. (c) Cobble-sized basalt clast at the snout of hyaloclastite mound. (d) Another view of the unsorted hyaloclastite deposit with accumulations of subrounded basalt clast. (e) A fining upwards sequence of hyaloclastite showing well developed foresets dipping towards the left of the image.

In thin section, the dyke shows well-developed euhedral, prismatic plagioclase phenocrysts compared to the pillows. There are also a few plagioclase-pyroxene glomeroporphyritic aggregates. The groundmass phases show sub-ophitic textures (Fig. 10a). The dyke shows porphyritic plagioclase crystals which are partly resorbed. In places and more towards the margin, plagioclase phenocrysts develop swallow-tailed morphologies (Fig. 10b). Slender lanceolate plagioclase is common in the groundmass (Fig. 10c). Abundance of chlorite (Fig. 10d) within the thin sections indicates that the dyke has been partly spilitized (Vallance, 1974a).

Compositionally, the plagioclases from the cores of the pillow are generally anorthitic, having ~An_{98} (Fig. 11a). Andesine (An_{34-45}) and oligoclase(An_{12-29}) are more common closer to the rim of the pillows. The plagioclase rims show the highest enrichment of Na, with most plagioclases in the pillow margins tending to albitic (An_{2-9}) compositions (Table S2). The pyroxenes within the pillows are classified as augites (Fig. 11b), varying in composition from $Wo_{26}En_{38}Fs_{36}$ to $Wo_{43}En_{46}Fs_{11}$. Plagioclases within the dyke core are labradorite in composition (An_{60-61}, Fig. 11a). In contrast, the margin of the dyke contains more Na-rich albitic plagioclases (An_{0-13}), indicating that they underwent albitization possibly under the influence of percolating seawater. There is also a population of K-rich pseudo-plagioclase crystals (Or_{91-97}), most likely due to gain in potassium from seawater interaction (keratophyrization). The augites from within the dyke plot as a distinct cluster on the pyroxene triangle (Fig. 11b) with compositions varying from $Wo_{44}En_{46}Fs_{10}$ to $Wo_{33}En_{55}Fs_{12}$.

Whole-rock geochemistry

All the samples analyzed from the present study plot within the sub-alkaline field of basalt in the TAS diagram (LeBas et al., 1986) and the Winchester and Floyd's (1977) Nb/Y vs. SiO_2 diagram (Fig. S4a, b). The normative mineralogy of the samples (Table 2) indicates the presence of hypersthene (which is expected for tholeiitic basalts) for all samples, except for CCPB, which is nepheline normative. The presence of normative nepheline in this sample is due to the much lower content of silica (47.91%), lost during spilitization (albitization) or relative gain in potassium during keratophyrization. In general, the sheet lavas show a higher Al_2O_3 (17.05 - 19.25 wt%) and K_2O (1.04 - 1.94 wt%) content with a lower MgO content (3.84 - 4.34 wt%). The Mg# (41.78 to 49.07) calculated for the sheet lavas are correspondingly much lower than the two pillow basalts (Mg# 56.37 and 62.06) and even the dyke sample (Mg# 65.40). In the Mg# vs. SiO_2 diagram (Fig. S4c), the samples show a positive correlation, while in the Mg# vs. Total alkali diagram (Fig. S4d), they show a negative correlation.

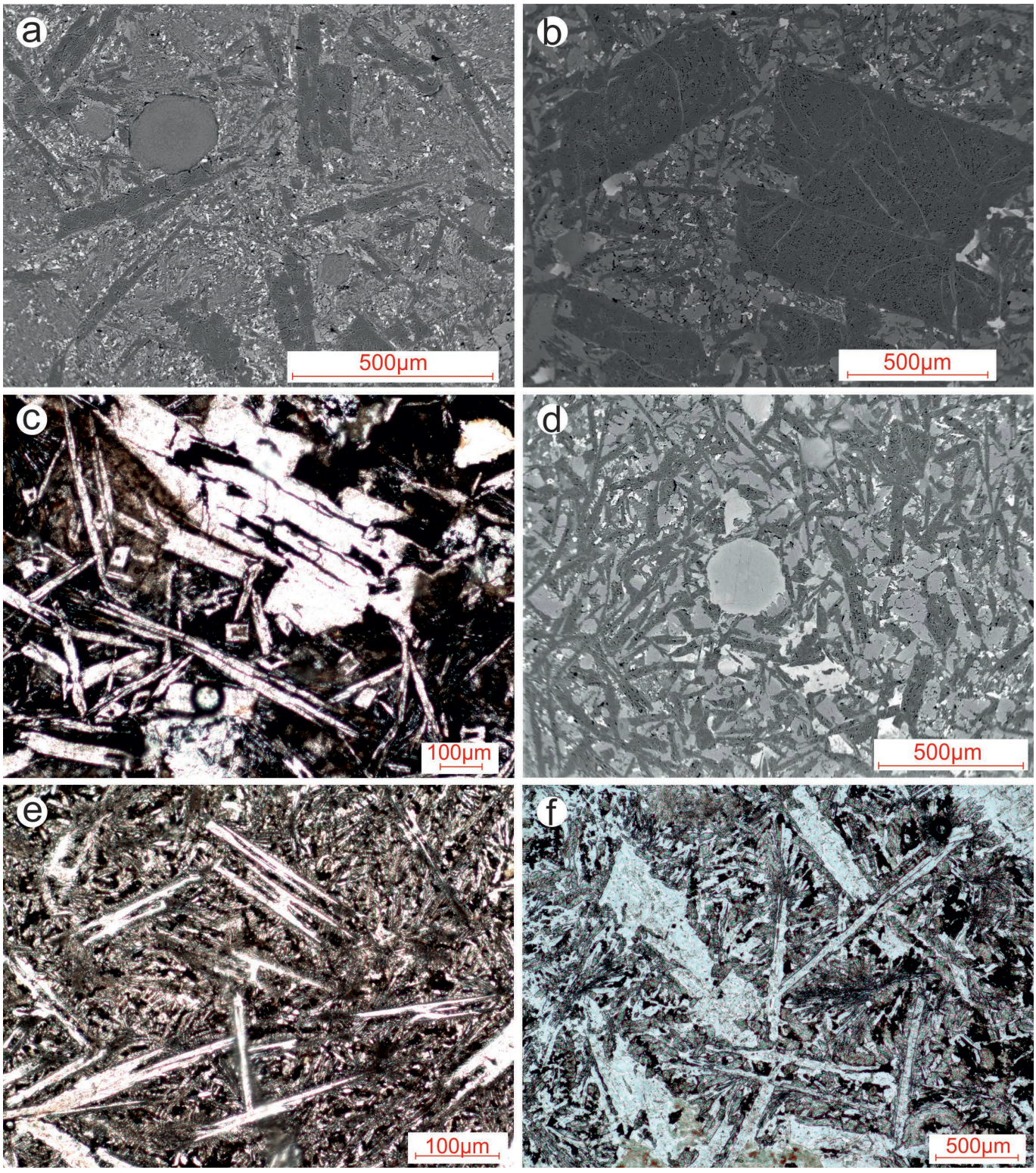

Fig. 8 - (a) BSE image showing prismatic plagioclase phenocrysts in fine groundmass. (b) Unzoned, blocky plagioclase phenocrysts in the interior of pillow. (c) Microporhyritic aggregates of earlier formed lath-shaped plagioclase crystals compared to the slender, swallow-tailed and acicular quenched plagioclase in the holohyaline groundmass. Many of the plagioclase microphenocryst cores appear to be resorbed with 'hopper' like forms in the center of the photograph. The groundmass is dominated by intersertal texture. Note the plagioclase 'bow-tie' fan spherulitic plagioclase below the hopper crystals. (d) BSE image depicting several acicular plagioclase crystals within glass in the groundmass. Note the spherical microvesicle in the centre. (e) Swallow-tail and H-shaped skeletal plagioclase crystals within a microcrystalline groundmass. (f) Heterogenous nucleation of pyroxene upon plagioclase. The pyroxenes depict a plumose texture indicating that they quenched rapidly. All photomicrographs (c, e, f) in plane polarized light.

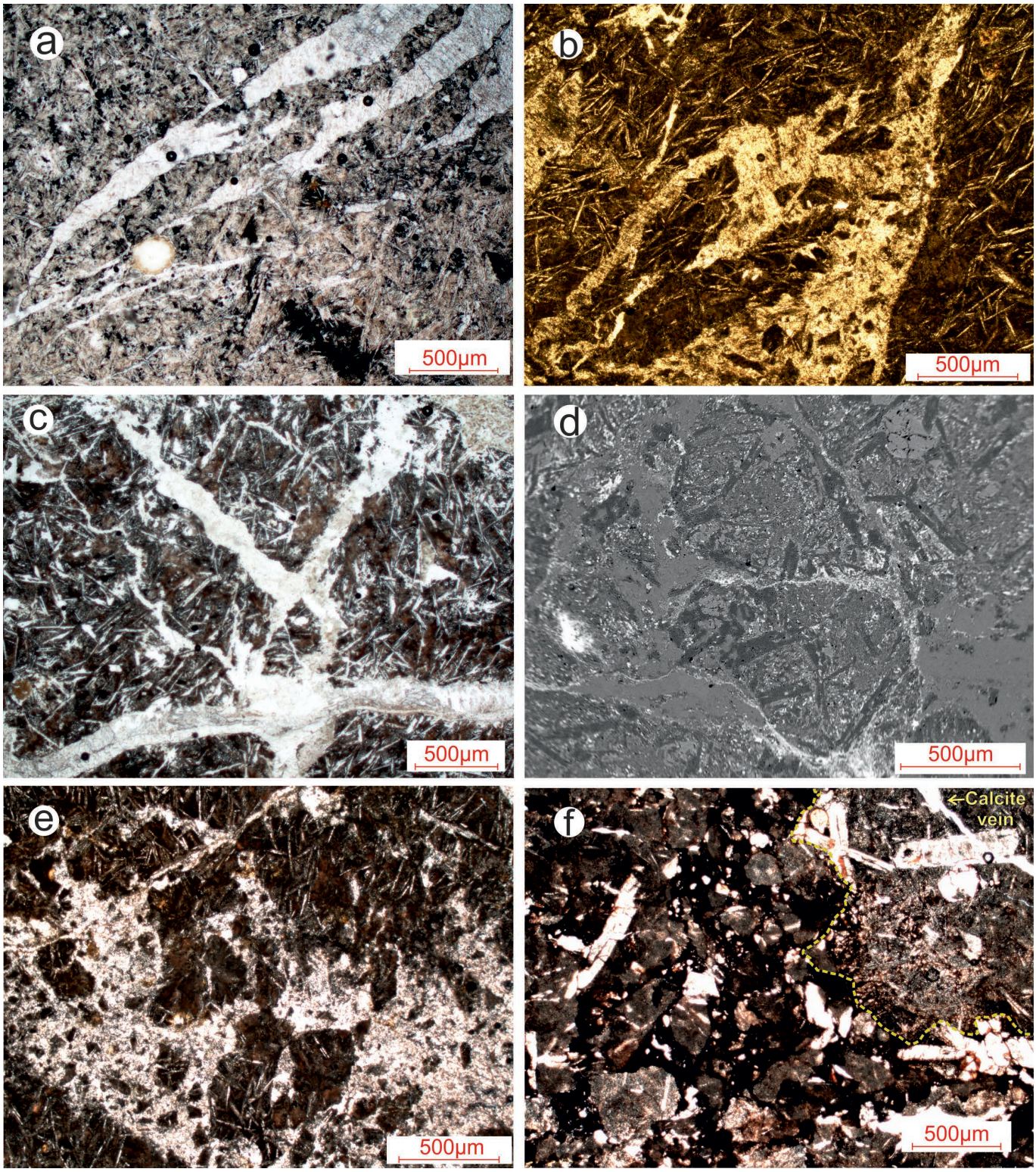

Fig. 9 - Photomicrographs of pillow-hyaloclastite. (a) Inflation crease or stretch marks within outer parts of pillow lobe. (b) Another view of fracturing and brecciation along inflation creases. Note the acicular quenched plagioclase fragments set within the glassy breccia fragments. (c) Propagation of criss-crossing fractures leading to intense brecciation within pillows. (d) BSE images of juvenile pillow fragments. (e) Hyaloclastite with breccia fragments of varying sizes within a calcite matrix. (f) Hyaloclastite containing basaltic fragments (highlighted by dashed yellow line) set within a devitrifying glassy matrix. In the top right corner, a calcite vein cuts across the plagioclase crystals suggesting that hydrothermal veining is subsequent to crystallization and quenching. All photomicrographs (a, b, c, e and f) in ppl.

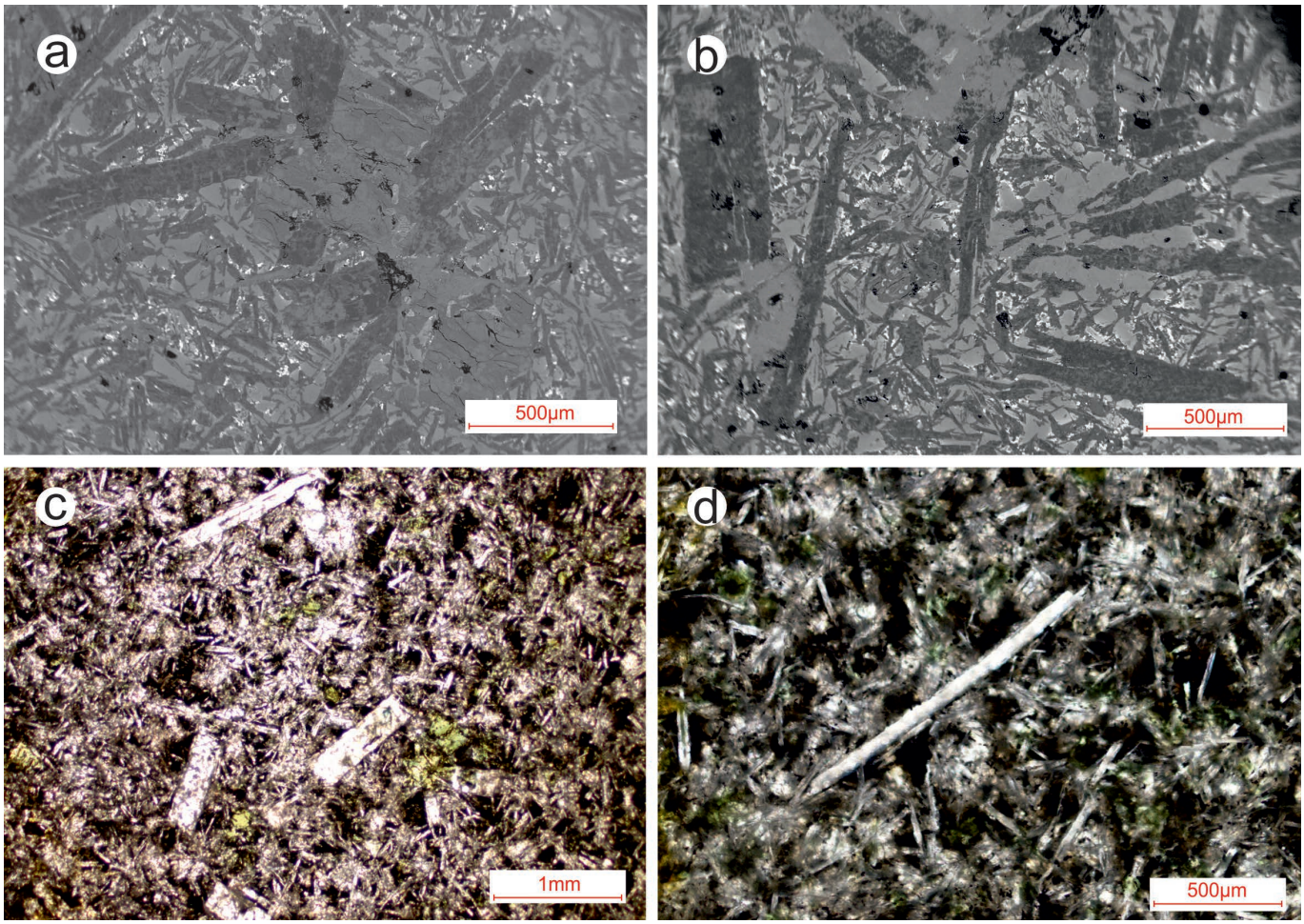

Fig. 10 - (a) BSE image depicting sub-ophitic texture between plagioclase and pyroxene microphenocrysts. (b) Plagioclase phenocryst within a fine-grained groundmass showing prismatic and swallow-tail terminations. Photomicrographs in PPL depicting (c) Partly reabsorbed plagioclase microphenocrysts set within a fine-grained, glassy groundmass containing a few grains of green chlorite. (d) Acicular plagioclase microphenocrysts set within a chloritized fine-grained groundmass.

Using the major element oxide data, three weathering indices i.e., Parker Index (Parker, 1970), Chemical Index of Alteration (CIA; Nesbitt and Young, 1982), and the Spitz-Darling Index of spilitization (S-D index; Spitz and Darling, 1978) were determined (Table 2). The Parker Index varies from 42.27 to 48.64 and suggests that the rocks are relatively fresh or indicate light weathering. In general, the CIA varies from 34.96 to 44.74. The CIA indicates that the sheet lavas are relatively fresh with variable degrees of alteration for the dyke and pillow lavas. The S-D Index varies from 4.93 to 7.98 and suggests variable degrees of spilitization. Based on the S-D Index, the dyke and pillows show higher degree of spilitization when compared to the thicker sheet lavas.

The sheet lavas show significantly higher concentrations of Rb (12.18 - 78.52 ppm), Sr (166 - 240.6 ppm), Zr (116.5 - 150.7 ppm), Nb (1.72 - 5.06 ppm), Cs (1.02 - 2.20 ppm), Ba (106.6 - 166 ppm), and Ce (20.48 - 21.08 ppm) than the pillow lava and dyke samples (Table 3). Similarly, MREE and HREE (e.g. Yb: 6.45 - 13.13 ppm; Lu: 0.46 - 0.99 ppm) are also significantly enriched in the sheet lavas. In the ternary AFM diagram (Fig. S5a), all samples plot within the tholeiitic field, except for the nepheline normative CCPB, which plots as calc-alkaline. In the normative feldspar diagram (Fig. S5b) of Yoder (1967), all the samples plot within the spilitized field. In the potassium number vs total alkali plot of Hughes (1973), the samples from the pillow lavas and dyke plot in the field of basalt while the sheet lavas tend to plot in the andesite field (Fig. S6), suggesting significant post-emplacement chemical modifications.

Various normalized spidergrams for the trace and rare earth elements (REEs) were plotted in order to assess the geochemical nature of the rocks. In the N-MORB (Sun and McDonough, 1989) normalized spidergram (Fig. 12a), positive anomalies are seen for Ce, Rb, U, K, Sr, P, Zr and Yb for all samples. A higher concentration of 10 to 100 times relative to that of the N-MORB concentration for Cs is also observed for these samples. Negative anomalies are observed for Th, Nb, Nd for all samples. The sheet lava samples specifically show positive anomalies for P and negative anomalies for Y. In the chondrite-normalized REE diagram (Nakamura, 1974), a positive anomaly is seen for Ce (Fig. 12b). The samples also show relatively high HREE contents. In general, the sheet lavas show a comparatively higher N-MORB, Chondrite-normalized trace and REE patterns compared to the pillow lavas and dyke.

Plagioclase mineral mapping

The compositional variations of major element oxides, using the SEM-ED XRF attachment, across two plagioclase phenocrysts (Plagioclase A and Plagioclase B, see Fig. 13a and Table S3) was undertaken to assess and evaluate alteration. The weathering indices calculated using bulk rock geo-

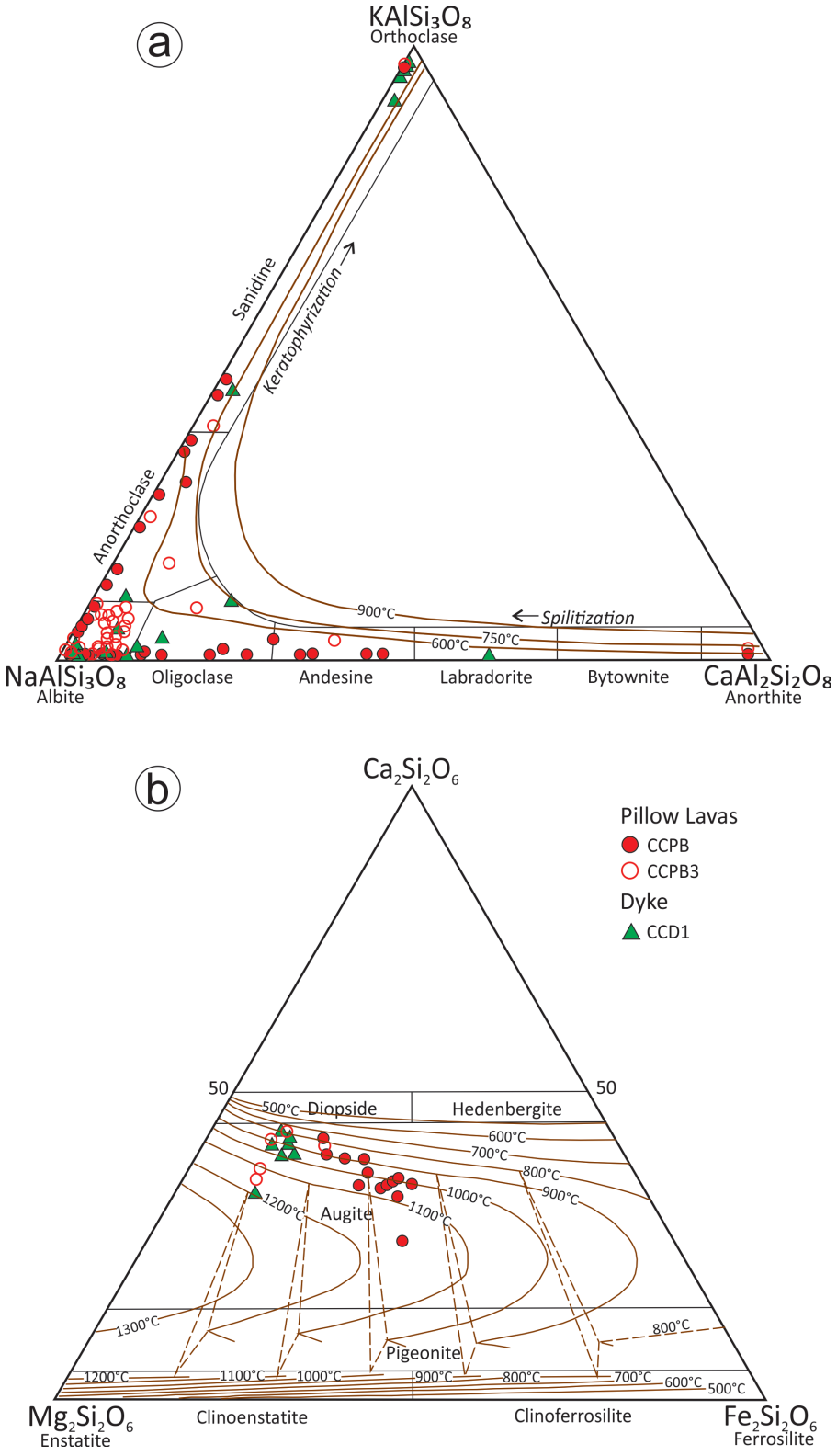

Fig. 11 - Ternary mineral classification plots for samples from Corbyn's Cove. (a) Plagioclase triangle ($NaAlSi_3O_8$-$KAlSi_3O_8$-$CaAl_2Si_3O_8$) for plagioclase and, (b) Hess's triangle ($MgSiO_3$-$FeSiO_3$-$CaSiO_3$) for pyroxene (nomenclature after Morimoto, 1988).

chemistry were calculated for these plagioclases. The CIA is particularly useful for characterising mineral alteration, since the theoretical value for a fresh plagioclase mineral is known to be 50 (Nesbitt and Young, 1982). The other indexes however, come with the caveat that these are all designed to quantify weathering within rocks, and therefore require bulk rock chemistry values, and not mineral values as has been used here. However, we believe that these parameters still provide useful insights into the different processes operating on the minerals analyzed and in the relative variations in weathering, alteration and spilitization that occur across the mineral profiles.

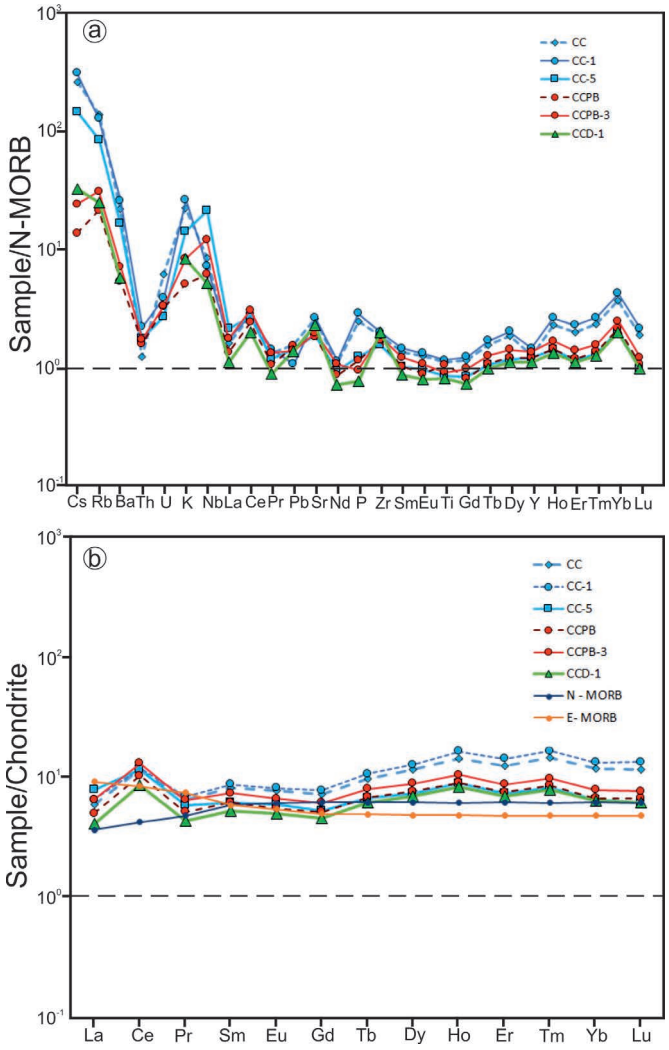

Fig. 12 - Trace element spidergrams normalized to (a) N-MORB (Sun and McDonough, 1989) (b) Chondrite (Nakumara, 1974).

The major oxide variations for Plagioclase A are shown in Fig. 13b. The central region of the Profile A (spots 6-10) shows relatively lower variations in all the major oxides plotted, with relatively lower proportion of silica and alumina and higher proportions of iron and magnesium with respect to the crystal rims. Towards the rim (outer portions of sites 6-10), higher proportions of sodium and potassium relative to the core are observed. The concentration of calcium remains low throughout the plagioclase phenocryst. The various chemical indices across Plagioclase A are shown in Fig. 13c. Lower values of the S-D index are seen for spots 1-5 and 11-13, indicating that these sites are more spilitized than the inner portion (sites 6-10). However, the high CIA and Parker index values for spots 6-10 indicate that they are altered. Based on these variations, we infer that sites 1-5 and 11-13 are spilitized, while sites 6-10 are altered.

Similarly, the major oxide variations for Plagioclase B are shown in Fig. 13d. The variations in major oxide are more unsystematic, with adjacent points showing greater degrees of variation, leading to a zig-zag variation pattern across the mineral. The aluminium content of the plagioclase shows the least amount of variation within the mineral. Sodium content of plagioclase remains low (< 1%), with significantly higher albitic portions noted at spots 5, 13 and 15. High iron and magnesium contents are recorded at spots 3, 6, 14 and 10-12. High calcium content is observed at spots 8 and 9. The various chemical indices across Plagioclase B are shown in Fig. 13e. Similar to the major oxide patterns, these indices also show a greater degree of variation compared to that of Plagioclase A. The regions of spilitization and alteration have been identified in different sites based on the variation in major oxides and the different chemical indices because of the complex variations across this profile. Where chemical indices offer conflicting information, major oxide variations were used directly, such as for site 4, which shows a relatively high S-D index, but a very high sodium content compared with calcium and potassium contents, indicating that this site is spilitized rather than altered despite the high Parker index and CIA. The mineral map for some elements across the spilitized and altered surface is presented in Fig. S7.

Geothermometry

Clinopyroxene composition and whole-rock geochemistry were used to calculate the temperatures using various models are presented in Table 4. Overall, the magmatic temperature of dyke ranges from 1222 to 1230°C which is higher than that recorded for pillow lavas (T = 1183 to 1218°C). These values are consistently and systematically lower in case of temperatures obtained from dykes using only clinopyroxene compositions (Table 4), and are comparable to temperatures obtained from isotherms (Fig 11b) of Lindsley (1983). In the ternary isotherm diagram of Seck (1971), the plagioclases from the dykes and pillows record temperatures of less than 750°C (Fig 11a) that can be attributed to rapid quenching and spilitization processes.

Table 4 - Geothermometric estimates of the dyke-pillow lavas samples.

		Based on whole rock + CPX compositions			Based on CPX compositions only	
Method		Putirka et al (1996)	Putirka (2008) RiMG MODELS		Nimis and Taylor 2000)	Putirka (2008) RiMG MODELS
Sample Number		Eqn T1 T(°C)	K_D(FeMg)	Eqn 34 T(°C)	T(°C)	Eqn. 32d T(°C)
CCD1	Cpx 1	1224.2	0.28	1198.9	1134.4	1198.8
n=8	Cpx 2	1221.5	0.28	1215.6	1028.2	1191.9
	Cpx 4	1236.7	0.29	1231	1088.4	1197.5
	Cpx 5	1237.4	0.29	1231	1122.5	1214.1
	Cpx 6	1223.7	0.28	1217.2	1054.3	1194.9
	Cpx 7	1235.5	0.29	1229.9	1071.6	1200.9
	Cpx 8	1230.6	0.29	1226.5	1054.7	1198.5
	Cpx 11	1234.6	0.29	1228.4	1096.6	1217
	Avg.	**1230.5**	**0.29**	**1222.3**	**1081.4**	**1201.7**
CCPB3	Cpx 5	1182.4	0.29	1177.1	1194.6	1201
n=4	Cpx 6	1190.1	0.3	1192.9	1056.6	1200.7
	Cpx 7	1193.9	0.36	1196.7	1013	1185.8
	Cpx 9	1174.5	0.3	1168.8	1161.3	1189.1
	Avg.	**1185.2**	**0.31**	**1183.9**	**1106.4**	**1194.2**
CCPB	Cpx 2	1189.7	0.47	1218.3	966.5	1168
n=4	Cpx 3	1191.1	0.47	1215.6	1022.8	1163.4
	Cpx 5	1194.9	0.5	1221.4	1002.4	**1162.6**
	Cpx 14	1191.4	0.49	1217.7	991.1	1162.3
	Avg.	**1191.8**	**0.48**	**1218.2**	**995.7**	**1164.1**

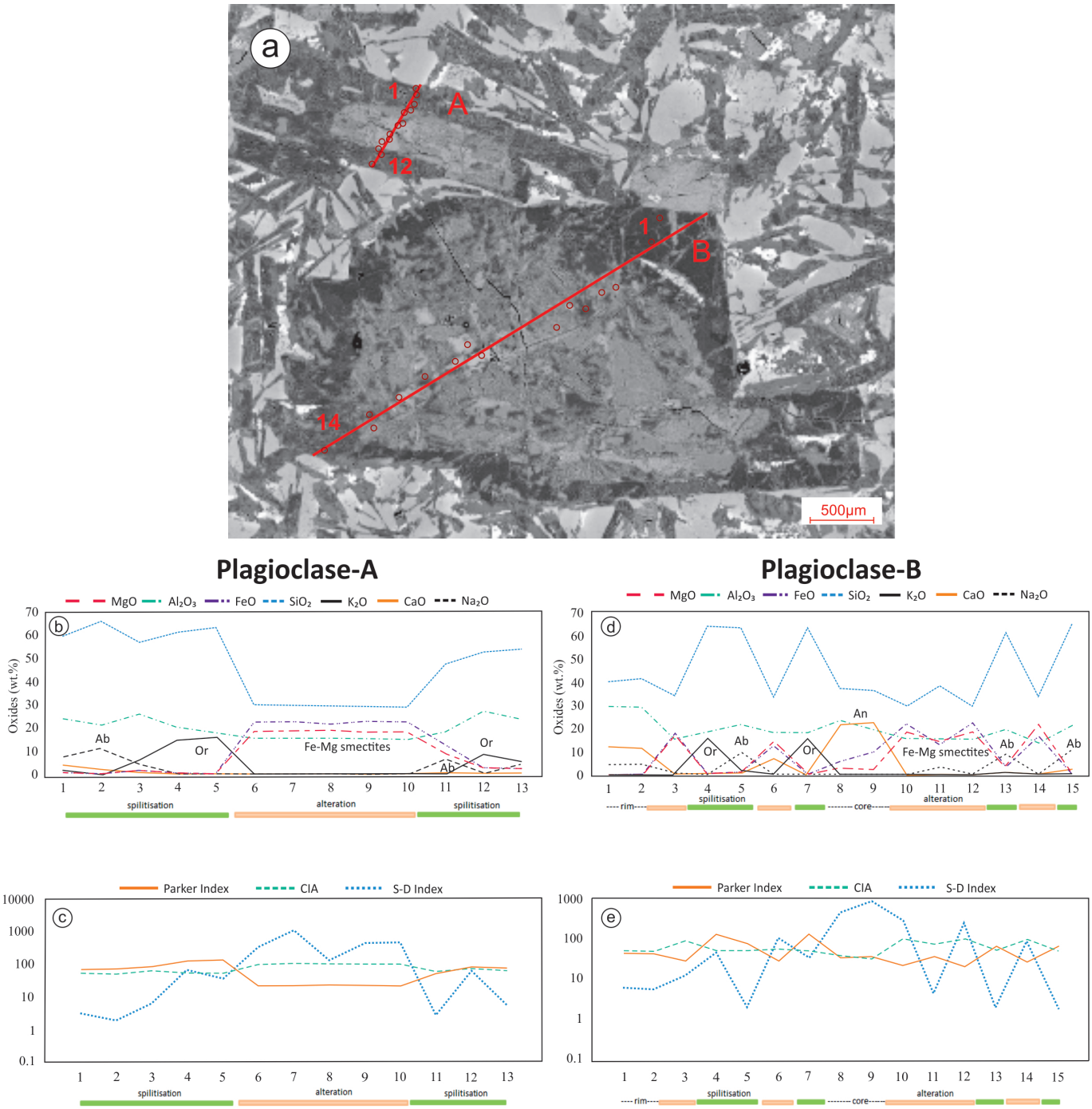

Fig. 13 - (a) BSE image depicting the two plagioclase phenocrysts. (Plagioclase-A at the top and Plagioclase-B at the bottom) across which compositional variations were analyzed (orange marks indicate analyzed spots). Profiles in graphs 'b' to 'e' generated from EPMA analyses. Major oxide variations (b) and weathering indices (c) for Plagioclase-A. Similarly, major oxide variations (d) and weathering indices (e) for Plagioclase-B.

DISCUSSION

The pillow lavas from the Corbyn's Cove section, Andaman and Nicobar Islands are argubably some of the best exposed from any Indian Ophiolite occurrence. Their unique morphology, internal structure and close association with the hyaloclastite deposits and submarine sheet lavas makes them worthy of preservation as a geoheritage site. Morphologically, the pillows from this site can be classified as dyke-fed pillowed lava flow (Walker, 1992). The physical volcanology, morphometry and petrochemical studies undertaken here provide a unique insight into the emplacement dynamics and environment of deposition of the pillow-hyaloclastite-sheet lavas along the Andaman Ophiolite belt.

Emplacement of the pillow-hayaloclastite-sheet lava sequence

We envisage that the entire dyke-pillow lava-sheet lava sequence from Corbyn's Cove area was emplaced subaqueously during the Late Cretaceous in the Indo-Sino Burmese context (Fig. 14a) along the flanks of a rising mid ocean ridge

(Fig. 14b). The geochemistry of the pillow-hyaloclastite sequence in the present study indicates a MORB origin, forming a part of the ocean floor prior to the Indo-Burmese collision. P-T estimates (1222 to 1230°C; 6 to 8 kbar, not reported in table) suggest that the magma was generated at shallow depths (~ 20 km) and were transported to the surface by dykes that fed the pillow lava flow fields (Fig. 14c). The distinct lack of vesicles in the pillow lobes suggests that they were emplaced at depths greater than 4 km below mean sea level. The combined low rate of effusion and high hydrostatic pressure that exists at this depth prevented individual pillow lobes from inflating too much, restricting them to bulbous forms with limited size spectrum. Further, the pillows quenched rapidly and did not develop any transverse or longitiudinal expansion cracks. The small pillow size, limited crust thickness, development of concentric and radial joints further prevented the lava from being insulated and allowed for efficient and violent heat loss along with quenching. Such a rapid heat loss, could then lead to the pillows imploding to various degrees, giving rise to the associated pillow breccia and hyaloclastite deposits. Evidence of hyaloclastite having phantom pillow forms lend credence to this fact. The craggy surfaces of most pillows could also be a function of quenching and crackling. The hyaloclastite deposits associated with the pillows are distinctly fine-grained and are also poorly sorted. In places, the hyaloclastite also exhibits normal size gradation, suggesting that these deposits flowed under the influence of gravity, similar to deposits formed in a prograde deltaic facies.

The physical morphology and internal structure of lava flows generally depends on its viscosity, its cooling rate, its effusion rate and the slope of the surface upon which the lavas are emplaced. Under similar conditions, if the effusion rate of the lava is higher, or if the slope is greater, the lavas will be emplaced as pāhoehoe sheets. Lower effusion rates and/ or slopes will give rise to individual pillow lobes (Gregg and Fink, 1995; 2000). Based on this, the smooth surfaced sheet lavas on top of the pillows (Fig. 1c) from the Corbyn's Cove area are indicative of emplacement at higher effusion rates under submarine conditions. Similar sheet lavas are common from the Galapagos rift, East Pacific Rise (Lonsdale, 1977; Ballard et al., 1979; Clague et al., 2009) and Atlantic Ocean (DSDP 52, Bryan et al., 1977) as well as in ancient greenstone belts (e.g., Duraiswami et al., 2013). Pockets and patches of coarse hyaloclastites within the crust of the sheet lavas also supports the fact that the sheets were emplaced below water. The sheet lavas are criss-crossed by a stockwork of calcite veins (Fig. 14d), some of which are also seen within individual hyaloclasts (but not the matrix), indicating that these calcite veins were almost sygenetic to the lava emplacement. By Late Miocene the ophiolite sequence were accreted on the south Andaman Islands (Fig. 14e) where they are presently exposed.

Syn-emplacement spilitic degradation

Pillow lavas and associated hyaloclastite deposits are highly altered due to sea floor hydrothermal processes or subsequent regional metamorphism and their geochemistry does not reflect the original composition of the erupted lavas (Hart et al., 1974; Baragar et al., 1979; Ludden and Thompson, 1979; Ludden et al., 1982; Staudigel and Hart, 1983; Alt, 1999; Polat et al., 2003). The lavas analyzed in the present study show at least two types and generations of alteration, indicating large post-emplacement changes in geochemistry.

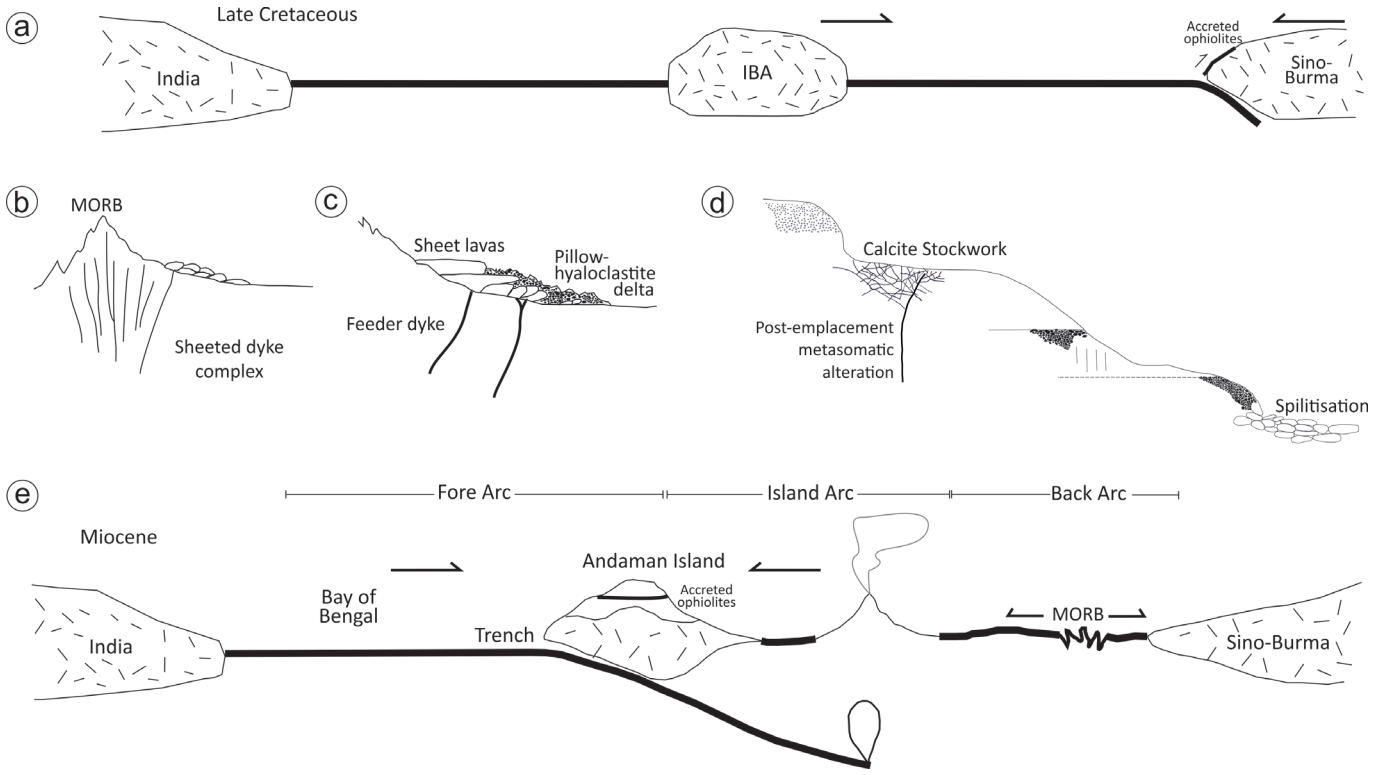

Fig. 14 - Cartoon depicting the stages in the formation and emplacement of dyke-pillow-hyaloclastite-sheet lava sequence. (a) Late Cretaceous tectonic setting of the Indo-Sino Burmese plates (b-d) emplacement of dyke-pillow lava-hyaloclastite- sequence. (e) Configuration of the Indo-Sinoburmese plates during Late Miocene. Note the development of the Andaman Island arc represented by the Narcondam and Barren volcanoes and the back arc setting. Cartoon 'a' and 'e' modified from Acharyya (2007).

Prolonged interaction of the basalt with circulating sea water gives rise to base-exchange that transforms basalt into spilite. Such alteration is seen in modern oceanic crust as well as in ancient basalts. Lava quench textures, presence of albite-chlorite assemblage (Fig. 10c, d), characteristic high sodium: potassium ratios and nepheline-normative compositions in some sample studied indicate that the pillow lavas and hyaloclastite from Corbyn's Cove have undergone variable degress of spilitic degradation (Cann, 1969). In spilitized basalts, calcium is selectively leached out from within the plagioclase, but pyroxenes remain in a metastable state, close to their original compositions (Vallance, 1974b). The salinity of the Andaman Sea provided the alkaline pH conditions conducive to base-leaching and hydrolysis during tholeiite-spilite transition. Based on geothermometric estimate, we presume that spilitization of the pillow lavas occurred at temperatures between 1218 to 1164ºC and lower.

Vallance (1974a) demonstrated that there is significant loss in SiO_2, CaO, FeO, Na_2O and Al_2O_3 and relative increase in MgO, Fe_2O_3 and CO_2 during spilitization of tholeiite lavas. The samples from Corbyn's Cove show loss in oxide percentage for SiO_2, CaO, MgO, and relative increase in FeO_T, Na_2O, K_2O, Al_2O_3, TiO_2 and P_2O_5. Such an unusual behaviour in geochemistry (especially in the sheet lavas) cannot be attributed to spilitization alone and an additional process of hydrothermal alteration is envisaged.

Hydrothermal alterations

Berger et al. (1988) found that Rb and Cs are preferentially incorporated within chlorites, smectites and analcite during the interaction of basaltic melts and rocks with seawater at temperatures ranging from 50 to 300°C. The trace element patterns observed for samples in the present study show a high relative enrichment of these elements, implying that the rocks were subjected to a phase of seafloor alteration as well after spilitization. This is also confirmed through the plagioclase mineral profiles discussed in the earlier section. In general, the trace element patterns for the lavas show patterns similar to that expected from N-MORBs, except for enriched LREEs and LILEs such as Cs, Rb Ba, U, K, Nb, and to a lesser extent some HREE (e.g., Yb). Enrichment of these elements is commonly seen as a result of seafloor alteration of basalts (Hart 1969; Hart et al., 1974; Philpotts et al., 1969). We attribute the peculiar trace element enrichment to a combination of syn-emplacement alkaline hydrothermal solutions and subsequent sea floor alteration. Thus, based on data from the present study, we conclude that the chemistry of the lavas has been significantly affected by spilitization and alteration.

CONCLUSIONS

The volcanic suite of South Andaman Ophiolite, India consists of a ~30 m thick sequence of sheet lava, pillows and hyaloclastite deposits in the Corbyn's Cove area of south Andaman Island. The tabular sheet lavas exposed in the top of the sequence are criss-crossed by a network of calcite veins and are hydrothermally altered. The pillows at the base of the sheet lavas constitute a modest flow field fed by dykes. Fairly thick hyaloclastite deposits containing sporadic patches of pillow breccias are intricately associated with the pillows in mound-like progradational bird foot deltas. The original magma was a MORB-like thoeliite.This dyke-pillow-hyalocastite assocciation has undergone various degrees of syn-emplacement spilitization and seafloor alteration. This study has clearly demonstrated that the geochemistry of the basaltic rocks from the South Andaman ophiolite are significantly affected by spilitization and hydrothermal alteration and as such may provide erroneous inferences about their petrogenesis as well as tectonic setting. Physical volcanology as well as detailed petrochemistry are therefore imperative in deciphering the true nature of submarine pillow-hayaloclastite-sheet lava sequences.

ACKNOWLEDGMENTS

We dedicate this paper to late Prof. Hiromitsu Yamagishi who always encouraged us to work on pillow lavas. We thank Prof. S.C. Patel for providing EPMA analyses, BSE images and elemental mapping at the National Facility, Indian Institute of Technology Powai, Mumbai. We thank Dr. Satyanarayan, National Geophysical Research Institute (NGRI), Hyderabad for ICP-MS analyses. The paper benefitted from the constructive reviews of Valentin Basch and Biswajit Ghosh. We also thank Alessandra Montanini, Editor and Staff of Ofioliti for all their support.

REFERENCES

Acharyya S.K., 2007. Collisional emplacement history of the Naga-Andaman ophiolites and the position of the eastern Indian suture. J. Asian. Earth. Sci., 29: 229-242.

Alt J.C., 1999. Hydrothermal alteration and mineralization of oceanic crust: mineralogy, geochemistry, and processes. In: C.T. Barrie, M.D. Hannington (Eds.), Volcanic-associated massive sulphide deposits: Processes and examples in modern and ancient settings. Rev. Econ. Geol., 8: 133-155.

Ballard R.D., Holcomb R.T., Andel V. and Tjeerd H., 1979. The Galapagos Rift at 86°W: 3. Sheet flows, collapse pits, and lava lakes of the rift valley. J. Geophys. Res., 84 (B10): 5407-5422.

Bandyopadhyay D., Ghosh B., Guilmette C., Plunder A., Corfu F., Advokaat E.L., Bandopadhyay P.C. and van Hinsbergen D.J.J., 2021. Geochemical and geochronological record of the Andaman Ophiolite, SE Asia: From back-arc to forearc during subduction polarity reversal? Lithos, 380-381:105853.

Bandyopadhyay D., van Hinsbergen D.J.J., Plunder A., Bandopadhyay P.C., Advokaat E.L., Chattopadhaya S., Morishita T. and Ghosh B., 2020. Andaman ophiolite: an overview. In: J.S. Ray and M. Radhakrishna (Eds.), The Andaman Islands and adjoining offshore: Geology, tectonics and paleoclimate. IGC Vol. under the Soc. Earth Scient. Series. Springer Intern. Publ., 400:1-17.

Baragar W.R.A., Plant A.G., Pringle G.J. and Schau M., 1979. Diagenetic and post diageneticchanges in the composition of an Archean pillow. Can. J. Earth Sci., 16: 2102-2121.

Berger G., Schott J. and Guy C., 1988. Behavior of Li, Rb and Cs during basalt glass and olivine dissolution and chlorite, smectite and zeolite precipitation from seawater: experimental investigations and modelization between 50 and 300°C. Chem. Geol., 71 (4): 297-312.

Bhattacharya S., Pande K., Kumar A., Kingson O. and Ray J. S., 2020. Timing of Formation and Obduction of the Andaman Ophiolite. In: J.S. Ray and M. Radhakrishna (Eds.), The Andaman Islands and adjoining offshore: Geology, tectonics and paleoclimate. IGC Vol. under the Soc. Earth Scient. Series. Springer Intern. Publ., 400: 19-42.

Bryan W.B., Robinson P.T. and White S.M., 1977. Studying oceanic layers. Geotimes, 22: 22-26.

Cann J.R., 1969. Spilites from the Carlsberg ridge, Indian ocean. J. Petrol., 10 (1): 1-19.

Clague D.A., Paduan J.B. and Davis A.S., 2009. Widespread strombolian eruptions of midocean ridge basalt. J. Volcan. Geotherm. Res., 180: 171-188.

Curray J.R., 2005. Tectonics and history of the Andaman Sea region. J. Asian Earth Sci., 25: 187-232. https://doi.org/10.1016/j.jseaes.2004.09.001

Duraiswami R.A., Inamdar M.M. and Shaikh T.N., 2013. Emplacement of pillow lavas from the ~ 2.8 Ga Chitradurga Greenstone Belt, South India: A physical volcanological, morphometric and geochemical perspective. J. Volcan.. Geotherm. Res., 264: 134-149. https://doi.org/10.1016/j.jvolgeores.2013.08.002

Duraiswami R.A., Jutzeler M., Karve A.V., Gadpallu P. and Kale M.G., 2019. Subaqueous effusive and explosive phases of late Deccan volcanism: evidence from Mumbai Islands, India. Arab. J. Geosci., 12: 1-21. https://doi.org/10.1007/s12517-019-4877-z

Ghosh B., Bandyopadhyay D., and Morishita T., 2017. Andaman-Nicobar ophiolites, India: Origin, evolution and emplacement. In: P.C. Bandopadhyay and A. Carter (Eds.), The Andaman-Nicobar accretionary ridge: Geology, tectonics and hazards, Geol. Soc. London Mem., 47: 95-110.

Ghosh B., Mukhopadhyay S., Morishita T., Tamura A., Arai S., Bandyopadhyay D., Chattopadhaya S. and Ovung T.N., 2018. Diversity and evolution of suboceanic mantle: constraints from Neotethyan ophiolites at the eastern margin of the Indian plate. J. Asian Earth Sci., 160:67-77.

Ghosh B., Pal T., Bhattacharya A. and Das D., 2009. Petrogenetic implication of ophiolitic chromite from Rutland Island, Andaman - a boninitic parentage in supra-subduction setting. Miner. Petrol., 96:59-70.

Gregg T.K. and Fink J.H., 1995, Quantification of submarine lava-flow morphology through analog experiments, Geol., 23(1): 73-76.

Gregg T.K. and Fink J.H., 2000. A laboratory investigation into the effects of slope on lava flow morphology, J. Volcanol. Geotherm. Res., 96(3-4): 145-159.

Gupta S., Borah K. and Saha G., 2016. Continental like crust beneath the Andaman Island through joint inversion of receiver function and surface wave from ambient seismic noise, Tectonophysics, 687: 129-138.

Hamilton W., 1978. Tectonic map of the Indonesian region, Map I-875-D. Dep. Inter. U.S. Geol. Surv.

Hamilton W., 1979. Tectonics of the Indonesian region. U.S.Geol. Surv. Prof. Pap., 1078: 1-308.

Hart S.R., 1969. K, Rb, Cs contents and K/Rb, K/Cs ratios of fresh and altered submarine basalts, Earth Planet. Sci. Lett. 6: 295-303.

Hart S.R., Erlank A.J. and Kable E.J.D., 1974. Sea-floor basalt alteration: some chemical and isotopic effects. Contrib. Miner. Petrol.. 44: 219-230.

Hughes C.J., 1973. Spilite, keratophyres and igneous spectrum, Geol. Mag., 109: 513-527.

Jafri S.H., Sarma D.S. and Sheikh J.M., 2010. Hyaloclastites in pillow basalts, South Andaman Island, Bay of Bengal, India. Curr. Sci., 99: 1825.1829. https://doi.org/10.2307/24073508

Jafri S.H. and Sheikh J.M., 2013. Geochemistry of pillow basalts from Bompoka, Andaman-Nicobar islands, Bay of Bengal, India. J. Asian Earth Sci., 64: 27-37. https://doi.org/10.1016/j.jseaes.2012.11.035

Karunakaran C., 1968. Tertiary sedimentation in the Andaman-Nicobar geosyncline. J. Geol. Soc. India,, 9: 32-39.

LeBas M., LeMaitre R., Streckeisen A. and Zanettin B., 1986. A chemical classification of volcanic rocks based on the total alkali-silica diagram. J. Petrol., 27: 745-750.

Lindsley D.H., 1983. Pyroxene thermometry. Am Miner., 68: 477-493.

Lonsdale P., 1977. Abyssal pahoehoe with lava coils at the Galapagos rift. Geology, 5: 147-152.

Ludden J., Gelinas L. and Trudel P., 1982. Archean metavolcanics from the Rouyn-Noranda district, Abitibi greenstone belt, Quebec. 2. Mobility of trace elements and petrogenetic constraints. Can. J. Earth Sci., 19: 2276-2287.

Ludden J.N. and Thompson G., 1979. An evaluation of the behaviour of the rare earth elements during the weathering of sea-floor basalts. Earth Planet. Sci. Lett., 43: 85-92.

Moore J.G., 1965. Petrology of deep-sea basalts near Hawaii. Am. J. Sci., 263: 269-277.

Morimoto N., 1988. Nomenclature of Pyroxenes. Miner. Petrol., 39: 55-76.

Nakumara N., 1974. Determination of REE, Ba, Fe,Mg, Na, and K in carbonaceous and ordinary chondrites. Geochim. Cosmochim. Acta, 38: 757-775.

Nesbitt H. and Young G.M., 1982. Early Proterozoic climates and plate motions inferred from major element chemistry of lutites, Nature, 299: 715-717.

Nimis P. and Taylor W.R., 2000. Single clinopyroxene thermobarometry for garnet peridotites. Part 1 Calibration and testing of a Cr-in-cpx barometer and an enstatite-in-cpx thermometer. Contrib. Miner. Petrol., 139: 541-554.

Pal T. and Bhattacharya A., 2010. Greenschist-facies sub-ophiolitic metamorphic rocks of Andaman Islands, Burma-Java subduction complex. J. Asian Earth Sci., 39: 804-814. https://doi.org/10.1016/j.jseaes.2010.05.017

Pal T., Chakraborty P.P., Gupta T.D. and Singh C.D., 2003. Geodynamic evolution of the outer-arc-forearc belt in the Andaman Islands, the central part of the Burma-Java subduction complex. Geol. Mag., 140: 289-307. https://doi.org/10.1017/S0016756803007805

Pal T., Dutta Gupta T., Chakraborty, P.P., Dasdupta, S.C. 2005. Pyroclastic deposits of Mio-Pliocene age in the Arakan Yoma-Andaman-Java subduction complex, Andaman Islands, bay of Bengal, India. Geochem. J., 39: 69-82. https://doi.org/10.2343/geochemj.39.69

Parker A., 1970. An index of weathering for silicate rocks. Geol. Mag., 107(6): 501-504.

Philpotts J.A., Schnetzler C.C. and Hart S.R., 1969. Submarine basalts: some K, Rb, Sr, Ba, rare-earth, H_2O, and CO_2 data bearing on their alteration, modification by plagioclase, and possible source materials, Earth Planet Sci. Lett., 7(3): 293-299.

Polat A., Hofmann A.W., Unker C.M., Regelous M. and Appel, P.W.U., 2003. Contrasting geochemical patterns in the 3.7-3.8 Ga pillow basalt cores and rims, Isua greenstone belt, Southwest Greenland: implications for postmagmatic alteration processes. Geochim. Cosmochim Acta, 67 (3): 441-457.

Putirka K., 2008. Thermometers and barometers for volcanic systems. In: K. Putirka and F. Tepley (Eds.), Minerals, inclusions and volcanic processes, Rev. in Miner. Geochem., Miner. Soc. Am., 69: 61-120.

Putirka K., Johnson M., Kinzler R. and Walker D., 1996. Thermobarometry of mafic igneous rocks based on clinopyroxene-liquid equilibria, 0-30 kbar. Contrib. Miner. Petrol., 123: 92-108.

Ray K.K., Sengupta S. and Van Den Hul H.J., 1988. Chemical characters of volcanic rocks from Andaman ophiolite, India. J. Geol. Soc London, 145: 393-400. https://doi.org/10.1144/gsjgs.145.3.0393

Seck H.A., 1971. Der Einfluß des Drucks auf die Zusammensetzung Koexistierender Alkalifeldspate und Plagioclase im System $NaAlSi_3O_8$-$KAlSi_3O_8$-$CaAl_2Si_2O_8$. Contrib. Miner. Petrol., 31: 67-86.

Sheth H.C., Ray J.S., Bhutani R., Kumar A. and Smitha R.S., 2009. Volcanology and eruptive styles of Barren Island: an active mafic stratovolcano in the Andaman Sea, NE Indian Ocean. Bull. Volcan., 71 (9): 1021-1039.

Spitz G. and Darling R., 1978. Major and minor element lithogeochemical anomalies surrounding the Louvem copper deposit, Val d'Or, Quebec, Can. J. of Earth Sci., 15(7): 1161-1169.

Srivastava R.K., Chandra R. and Shastry A., 2004. High-Ti type N-MORB parentage of basalts from the south Andaman ophiolite suite, India. Proceed. Indian Acad. Sci., Earth Planet. Sci., 113: 605-618. https://doi.org/10.1007/BF02704025

Staudigel H. and Hart S.R., 1983. Alteration of basaltic glass: mechanism and significance for the oceanic crust-seawater budget. Geochim. Cosmochim. Acta, 47: 337-350.

Subrahmanyam C., Gireesh R., Chand S., Raju, K.K. and Rao, D.G., 2008. Geophysical characteristics of the Ninetyeast Ridge-Andaman island arc/trench convergent zone, Earth Plan. Sci. Lett. 266(1-2): 29-45.

Sun S.S. and McDonough W.F., 1989. Chemical and isotopic systematics of oceanic basalts: Implications for mantle composition and processes. Geol. Soc. London Spec. Publ., 42: 313-345. https://doi.org/10.1144/GSL.SP.1989.042.01.19

Vallance T.G., 1974a. Spilitic degradation of a tholeiitic basalt, J. Petrol. 15(1): 79-96.

Vallance T.G., 1974b. Pyroxenes and the Basalt. Spilite relation. In: G.C. Amstutz (Eds.), Spilites and spilitic rocks Springer, Berlin, Heidelberg, 1: 59-68.

Verma S.P., Torres-Alvarado I.S. and Sotelo-Rodríguez, Z.T., 2002. SINCLAS: standard igneous norm and volcanic rock classification system, Comp. Geosci. 28(5): 711-715.

Winchester J.A. and Floyd P.A., 1977. Geochemical discrimination of different magma series and their differentiation products using immobile elements, Chem. Geol. 20: 325-343.

Walker, G.P.L., 1992. Morphometric study of pillow-size spectrum among pillow lavas. Bull. Volcan., 54: 459-474. https://doi.org/10.1007/BF00301392

Yamagishi H., Kawachi S., Goto Y., Miyasaka S., and Koitabashi, S., 1989. A Miocene Submarine Volcano: The Rekifune Volcanic Rocks in Southern Tokachi, Hokkaido. Sec. Ser. Bull. Volcanol. Soc. Japan, 34(4): 251-261.

Yoder H.S.J., 1967. Spilites and serpentinites. In: C.P. Haskins (Eds.), Year Books. Carnegie Inst. Washington, 65: 269-279.

Received, June 28, 2021
Accepted, September 6, 2021
First published online, September 27, 2021